Orbital-Dependent Charge Transfer Dynamics in Conjugated Self-Assembled Monolayers

H. Hamoudi, S. Neppl, P. Kao, B. Schüpbach, P. Feulner, A. Terfort, D. Allara, and M. Zharnikov

Phys. Rev. Lett. **107**, 027801 — Published 5 July 2011

DOI: 10.1103/PhysRevLett.107.027801

Orbital-dependent charge transfer dynamics in conjugated self-assembled monolayers

H. Hamoudi,[1] S. Neppl,[2] P. Kao[3], B. Schüpbach,[4] P. Feulner,[2] A. Terfort,[4] D. Allara,[3] and M. Zharnikov[1,*]

[1]*Angewandte Physikalische Chemie, Universität Heidelberg, 69120 Heidelberg, Germany*

[2]*Physikdepartment E20, Technische Universität München, 85747 Garching, Germany*

[3] *Departments of Chemistry and Material Science, Pennsylvania State University, University Park, PA 16802, USA*

[4] *Institut für Anorganische und Analytische Chemie, Universität Frankfurt, Max-von-Laue-Straße 7, 60438 Frankfurt, Germany*

Femtosecond charge transfer (CT) dynamics in a series of self-assembled monolayers with oligo(phenylenethynylene) and oligo(phenyl) backbone is addressed by resonant Auger spectroscopy using the core hole clock method. The characteristic CT times are found to depend strongly on the character of the molecular orbital (MO) which mediates the CT process. This demonstrates that the efficiency and rate of CT through molecular frameworks can be controlled by resonant injection of the charge carriers into specific MOs.

PACS numbers: 81.16.Dn, 78.70.Dm, 82.80.Pv, 73.61.Ph

Continued progress in technologically important fields such as molecular and organic electronics as well as organic photovoltaics depends on reliable information about the charge transport (CT) through individual molecular units [1,2] (or loosely, "molecular wires" - MWs) which serve as charge conduction paths between a charge injection site and an electrode connected to the molecule by an anchor group, typically via a chemical bond. Transport properties of potential MWs, both individual and configured in ensembles on a conductive substrate have been extensively studied both theoretically [2] and experimentally [3]. The experiments have provided data for the time-averaged, static CT properties of MWs. In most cases, these properties are well described by the equation, $R = R_0 \exp(+\beta l)$, where R is the overall resistance of a molecular junction, R_0 is the molecular contact resistance, β is an attenuation factor, and l is the length of the molecular backbone [2,4-9]. Such a behavior is associated with the nonresonant superexchange tunneling mechanism which involves tunneling through molecular orbitals (MOs) with the efficiency dependent on the internal coupling between the building units of the MW [2]. An alternative mechanism involves hopping between these units at a rate depending on the exact position of the mediating state with respect to MOs [2]. The values of β, which should be as small as possible for efficient CT, range from β ~0.2-0.3 $Å^{-1}$ for unsaturated hydrocarbon chains, such as oligo(phenylenethynylenes) (OPE; $\beta = 0.27$ $Å^{-1}$) [10] or oligophenyls (OPh, $\beta = 0.41$ $Å^{-1}$) [6], to ~0.6-1.0 $Å^{-1}$ for saturated chains such as alkanes [6]. These values describe, however, the overall performance of the bridging MWs and neither distinguish between the roles of individual MOs in the CT event nor provide information on the dynamics.

In this Letter, by the example of several molecules comprised of conjugated π-systems and arranged in self-assembled monolayers (SAMs) on Au(111), we demonstrate experimentally that the efficiency of CT through a MW can be strongly affected by the character of the involved MOs. In addition, in contrast to the majority of studies dealing with molecular conductivity, we address not the *static* CT properties of potential MWs but the CT *dynamics* in these systems.

To this end we applied the so-called core hole clock (CHC) method within the general framework of resonant Auger electron spectroscopy (RAES). This contact-free approach is based on the analysis of core hole decay spectra obtained for resonant core-to-bound excitation. The resulting spectra differ for decay events *before* and *after* the delocalization (CT) of the resonantly excited electron and can be decomposed into the respective contributions [11]. The CT time (τ_{CT}) can then be obtained from the relation $\tau_{CT} = \tau_{core}\ (1\text{-}P_{CT})/P_{CT}$, where τ_{core} is the known lifetime of inner shell vacancy and P_{CT} is the relative intensity of the post-CT portion in the total decay spectrum [11-14]. Since τ_{core} is just few fs for inner shell vacancies in atoms common to organic molecules, this approach offers time resolution in the fs and sub-fs range, in addition to atom-selective charge injection (see below).

Previously, the CHC method has been applied to potential MWs arranged in SAM fashion [15,16]. However, no quantitative information, beyond the observation of CT to the substrate itself, could be obtained since the excitation site was not unequivocally defined. This ambiguity was removed later by the attachment of a specific tail group which could be resonantly excited by X-rays [17]. In this way, the CT path through the backbone and across the headgroup-substrate anchor is unambiguously defined. As a suitable group, the nitrile (–C≡N) moiety was identified [17]. First experiments were performed on SAMs of alkanethiols (AT) on Au(111) [17,18]. It was shown that τ_{CT} for CT through the alkyl chain [–$(CH_2–)_n$] can be, similar to the static conductance, described by an exponential function with an attenuation factor of 0.72 $Å^{-1}$ (0.93 per CH_2) and a value of 2.3 fs for τ_{CT} across the thiolate-Au anchor [17,18].

In the present study we combined the nitrile tail group with the OPE and OPh chains of different lengths, which were attached either directly, or over a methylene unit, to the thiol headgroup. From these molecules (see Fig. 1), we prepared SAMs on Au(111) substrates (by immersion in 1 mM molecular solution in CH_2Cl_2 or toluene for 24 h), verified their quality by high-resolution

X-ray photoelectron spectroscopy and near-edge X-ray absorption fine structure (NEXAFS) spectroscopy, and performed the RAES measurements. The experimental conditions and the way the spectra were measured were identical to those of ref [19]. The energies for the resonant excitation of the nitrile functionality were determined by NEXAFS spectroscopy. The N K-edge NEXAFS spectra of NC-OPE1/Au, which is the shortest member of both OPE and OPh families, are presented in Fig. 2 along with the results of quantum-chemical calculations of the relevant molecular orbitals. These spectra and calculations are representative of all the molecules in this study. The spectrum acquired at an X-ray incidence angle of 55° reflects the electronic structure of NC-OPE1/Au while the difference between the spectra acquired at incidence angles of 20° and 90° is sensitive to the molecular orientation [20]. The 55° spectrum is dominated by a double resonance at ~398.8 and ~399.75 eV. This spectrum resembles that of benzonitrile [21,22] and is also typical of SAMs containing this group [19,23,24]. The appearance of the strong double resonance is related to the conjugation between the π* orbital of the nitrile group and the adjacent phenyl ring. As a result, the degeneracy of the former orbital is lifted and it splits into two states with different energies, polarized either perpendicular (π_1*) or parallel (π_3*) to the ring plane (see Fig. 2), in good agreement with the previous work [21,22]. The lower intensity of the π_1* resonance as compared to π_3* is related to the delocalization of the π_1* orbital over the entire benzonitrile moiety, whereas π_3* is localized on the nitrile group (see Fig. 2). The negative character of the π_1* and π_3* peaks in the difference spectrum suggests that the respective orbitals are oriented parallel to the substrate [23], implying an upright molecular orientation characteristic of all the SAMs in this study, even though the orientational order depends to some extent on the chain length and character.

By tuning the excitation energy, N1s electrons were excited selectively either into the π_1* or into the π_3* orbital at the location of the nitrogen atom. The resulting [N1s]π_1* and [N1s]π_3* RAES

spectra of the NC-OPE1, NC-OPE2, and NC-OPE3 SAMs are presented in Fig. 3, along with the non-resonant AES spectrum of NC-OPE1/Au. The individual features in the RAES spectra are assigned in accordance with the scenarios for the decay of the initially neutral core-excited state [17,18]. First, within the so-called participator (P) scenario, the excited electron itself takes part in the decay process leading to a one hole final state.. Second, within the so-called spectator (SP) scenario, the excited electron stays in the unoccupied valence states while two other electrons from occupied valence (OV) levels fill the hole and are emitted, respectively (two hole, one electron final state). Finally, if CT of the excited electron to the substrate occurs during the core hole lifetime, only the normal Auger decay channel (involving two OV electrons) is possible. The above scenarios result in differently charged final states, with one hole per excited molecule in integral in the P and SP cases and two holes in the CT case. The latter final state is identical to that of the Auger decay in the case of non-resonant excitation. Therefore, the appearance and intensity of the respective features (A1 and A2 in the bottom spectrum in Fig. 3) in the RAES spectra serves as a fingerprint and direct measure of CT.

A comparison of the resonant and non-resonant spectra in Fig. 3 suggests that there is no perceptible admixture of the A1 and A2 features in the resonant spectra of NC-OPE2/Au and NC-OPE3/Au. In addition, these spectra are practically identical to one another and to the analogous spectra of NC-TP1/Au (not shown) for both [N1s]π_1* and [N1s]π_3* cases. In view of the different molecular lengths and chemical compositions of the above molecules, it can only mean that the respective CT contributions are negligible and the spectral character is mostly determined by the common unit, viz. terminal benzonitrile moiety. Presumably, the characteristic CT time for NC-OPE2/Au and NC-OPE3/Au is much longer than the N1s core hole lifetime of 6.4 fs [25] and is therefore not resolvable within the applied CHC scheme. It is also possible that

CT did not occur because of energetic reasons [17] since the π_1* orbital in the above systems lies below the Fermi level of the substrate.

In contrast, the RAES spectra of NC-OPE1/Au exhibit an additional intensity at the positions of the characteristic features of the non-resonant spectrum, which is associated with an admixture of the CT contribution. We therefore fitted these spectra to linear combinations of the non-resonant spectrum and the blue-shifted RAES spectra of NC-OPE3/Au (either for the [N1s]π_1* or [N1s]π_3* case) which we assume to represent the "pure" autoionization spectra of the benzonitrile group. The results of these fits are presented in Fig. 4, along with the analogous fits for the RAES spectra of NC-PT1/Au and NC-BP0/Au. Note that NC-PT1 differs from NC-OPE1 by the $-CH_2-$ moiety inserted between the phenyl ring and thiol anchor while NC-BP0 represents the second successive (after NC-OPE1) member of the OPh family. Most significant, for all three SAMs in Fig. 4, the derived portions of the non-resonant contributions are noticeably higher for the [N1s]π_1* then for the [N1s]π_3* initial state, which indicates that CT via the π_1* orbital is much more efficient. It should be noted that this behavior cannot be explained by energetic considerations [17] since CT via the π_3* orbital is energetically more favorable due to its higher excitation energy as compared to the [N1s]π_1* case. Thus, it should be the conjugation of the molecular orbitals which is responsible for the difference in CT efficiency. Employing the basic formula of the CHC approach (see above), we found the following transfer times τ_{CT} of the resonantly excited electron from the CN tail group of the NC-OPE1 molecules to the substrate: 9±3 fs for [N1s]π_1* and 31.5±4.5 for [N1s]π_3*. For NC-PT1/Au, these values are 19.2±5 fs ([N1s]π_1*) and 60±10 fs ([N1s]π_3*); note the strong effect of insertion of a single CH_2 group. For NC-BP0/Au, only τ_{CT} at the [N1s]π_1* excitation could be measured (29±6 fs), whereas τ_{CT} for the [N1s]π_3* case was beyond the range accessible by the CHC approach in our experiments

(τ_{CT} < 120-150 fs). The [N1s]π_3* spectrum of NC-BP0/Au coincided with the analogous spectrum of NC-OPE3/Au (taken as a pure autoionization spectrum) and no non-resonant contribution was perceptible.

Considering that NC-OPE1 and NC-BP0 are the successive members of the OPh series and assuming that τ_{CT} through the OPh chain, similar to the alkyl one [18] and in accordance with the presumable CT mechanisms [2], can be described by the formula $\tau_{CT} = \tau_{S\text{-}Au} exp(\beta_{OPh} l_{OPh})$, we estimated the dynamic attenuation factor (β_{OPh}) for CT through the π_1* orbital from a $\ln\tau_{CT}$ vs. OPh chain length (l_{OPh}) plot. The respective value of β_{OPh} is 1.17 per phenyl ring (0.27 Å^{-1}; a tunneling along the chain was assumed) while the time associated with the CT across the thiolate anchor ($\tau_{S\text{-}Au}$) was found to be 2.8 fs which is very close to the analogous value for AT SAMs (2.3 fs) [18] utilizing the same anchor. The analogous procedure for the π_3*-mediated CT was not possible since the respective τ_{CT} for NC-BP0/Au lies beyond the access range of the CHC approach in our case. We therefore concentrated on the RAES data for NC-PT1/Au. Assuming that τ_{CT} for this system is described by the formula $\tau_{CT} = \tau_{S\text{-}Au} exp(\beta_A l_A) exp(\beta_{OPh} l_{OPh})$, where l_A and l_{OPh} are the lengths of the aliphatic and aromatic parts of the hybrid chain, β_A and β_{OPh} are the respective attenuation factors, and $\tau_{S\text{-}Au} exp(\beta_A l_A)$ is known from the previous work [18], we could calculate approximate values of β_{OPh} for both [N1s]π_1* and [N1s]π_3* cases. These values are 1.25 and 2.34 per phenyl ring (0.29 and 0.55 Å^{-1}), respectively. The first value is quite close to the corresponding value obtained from the joint evaluation of the NC-OPE1 and NC-BP0 data, which confirms the reliability of these values even though they are somewhat tentative. It is, of course, questionable to what extent these values, obtained for the excited state of vacuum exposed SAM molecules, are applicable to the standard situation of current flowing through a bridging molecule between opposing solid state electrodes. However, within a simple

phenomenological model, the dynamical CT data obtained within the CHC approach agree well with the static conductance data [17]. This can be tentatively explained by the assumption that the initial state of the tunnelling process governs the CT dynamics, which corroborates previous CHC results [11,14]. Considering that for the alkyl chain the static attenuation factor is quite close to the dynamic one [18], the derived β values for the OPh chain can also be compared to the respective static factor (0.67 $Å^{-1}$ [4], 0.41 $Å^{-1}$ [6], and 0.7 $Å^{-1}$ [8]). The latter values are closer to our π_3* value, which indicates indirectly that the static tunnelling in the respective experiments did not occur over the most suitable molecular orbital of OPh. This is not surprising since no special efforts in this direction were made.

In summary, using the CHC approach we have measured the characteristic CT times for a variety of OPE- and OPh-based molecules arranged in SAMs on a Au(111) substrate and demonstrated their strong dependence on the character of the MO which mediates the CT process. These results demonstrate experimentally that the efficiency of tunnelling in MWs can be significantly affected by controlling the specific orbitals into which charge carriers are injected. This can be a valuable input for theory and an important consideration for molecular electronics devices where improvements in conductance can have significant technological impact.

We thank the MAX-lab staff for technical assistance. This work has been supported by DFG (ZH 63/14-1) and the European Community's Seventh Framework Programme (FP7/2007-2013) under grant agreement Nº 226716 (HH and MZ), DFG through the graduate school 611 ("Functional materials") (BS and AT), the Munich Centre for Advanced Photonics (MAP C.1.5.) (SN and PF), and the NSF funded PSU Center for Nanoscale Science (MRSEC DMR 0080019) (PK and DA).

References

* To whom correspondence should be addressed: phone: +49-6221-54 4921, fax: +49-6221-54 6199, E-mail: Michael.Zharnikov@urz.uni-heidelberg.de

[1] J. M. Tour, *Molecular electronics*, World Scientific, Singapore, 2003.

[2] D.M. Adams *et al.*, J. Phys. Chem. B **107**, 6668 (2003).

[3] H. Haick and D. Cahen, Prog. Surf. Sci. **83**, 217 (2008).

[4] M. A. Rampi, O. J. A. Schueller, and G. M. Whitesides, Appl. Phys. Lett. **72**, 1781 (1998).

[5] E. A. Weiss *et al.*, J. Am. Chem. Soc. **129**, 4336 (2007).

[6] D. J. Wold *et al.*, J. Phys. Chem. B **106**, 2813 (2002).

[7] V. B. Engelkes , J. M. Beebe, and C. D. Frisbie, J. Am. Chem. Soc. **126**, 14287 (2004).

[8] A. V. Tivanski *et al.*, J. Phys. Chem. B **109**, 5398 (2005).

[9] B.-S. Kim *et al.*, *J. Am. Chem. Soc.* **128**, 4970 (2006).

[10] J. K.; Tomfohr and O. F. Sankey, Phys. Rev. B **65**, 245105 (2002).

[11] P. A. Brühwiler, O. Karis, N. Mårtensson, Rev. Mod. Phys. **74**, 703 (2002).

[12] J. Schnadt *et al.*, Nature **418**, 620 (2002).

[13] M. P.de Jong *et al.*, Phys. Rev. B **72**, 035448 (2005).

[14] A. Föhlisch *et al.*, Nature **436**, 373 (2005).

[15] W. Chen *et al.*, *J. Am. Chem. Soc.* **128**, 935 (2006).

[16] L. Wang *et al.*, J. Phys. Chem. B **110**, 674 (2006).

[17] S. Neppl *et al.*, *Chem. Phys. Lett.* **447**, 227 (2007).

[18] P. Kao *et al.*, J. Phys. Chem. C **114**, 13766 (2010).

[19] N. Ballav *et al.*, J. Phys. Chem. C **114**, 12719 (2010).

[20] J. Stöhr, *NEXAFS spectroscopy*; Springer Series in Surface Sience 25; Springer-Verlag, Berlin, 1992.

[21] S. Carniato *et al.*, Phys. Rev. A **71**, 022511 (2005).

[22] S. Rangan *et al.*, Phys. Rev. B **71**, 165318 (2005).

[23] N. Ballav *et al.*, J. Am. Chem. Soc. **129**, 15416 (2007).

[24] L. Hallmann *et al.*, Langmuir **24**, 5726 (2008).

[25] B. Kempgens *et al.*, J. Phys. B **29**, 5389 (1996).

Figure captions

FIG. 1. A schematic drawing of the SAM precursor molecules along with their acronyms.

FIG. 2. N K-edge NEXAFS spectra of NC-OPE1/Au; at the top: the spectrum acquired at an X-ray incidence angle of 55°; at the bottom: the difference between the spectra acquired at X-ray incident angles of 20° and 90°. The same vertical scale is used for both curves. The dotted line corresponds to zero. The dominant absorption resonances are assigned and the respective, calculated molecular orbitals are shown.

FIG. 3. [N1s]π_1* and [N1s]π_3* RAES spectra of NC-OPEn/Au, along with the non-resonant AES spectrum of NC-OPE1/Au. P, SP1, and SP2 denote the participator and two spectator features, respectively (the P feature is strongly suppressed in the [N1s]π_1* spectra; see ref 19 for a tentative explanation of this phenomenon). A1 and A2 denote two characteristic features in the non-resonant spectra. The kinetic energy ranges where a contribution from these features in the RAES spectra can be expected are highlighted by light gray.

FIG. 4. Reproduction (green lines) of the [N1s]π_1* (at the top) and [N1s]π_3* (at the bottom) RAES spectra of the NC-OPE1 (A), NC-PT1 (B), and NC-BP0 (C) SAMs (black lines) by the linear combination [17,18] of the resonant (blue lines) and non-resonant (red lines) contributions.

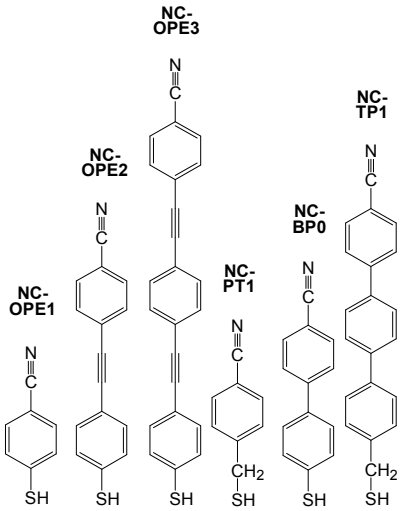

Figure 1

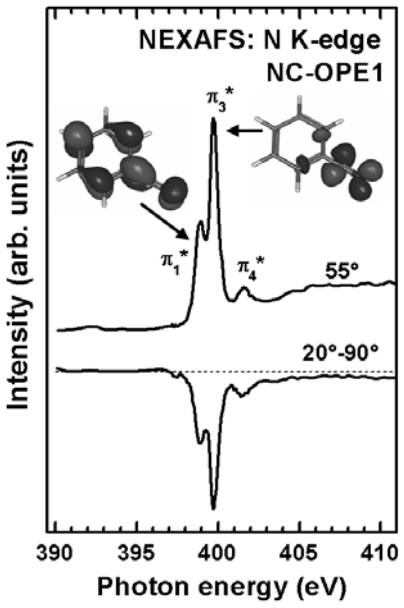
NEXAFS: N K-edge
NC-OPE1
π3*
π1*
π4*
55°
20°-90°
Intensity (arb. units)
390
395
400
405
410
Photon energy (eV)

Figure 2

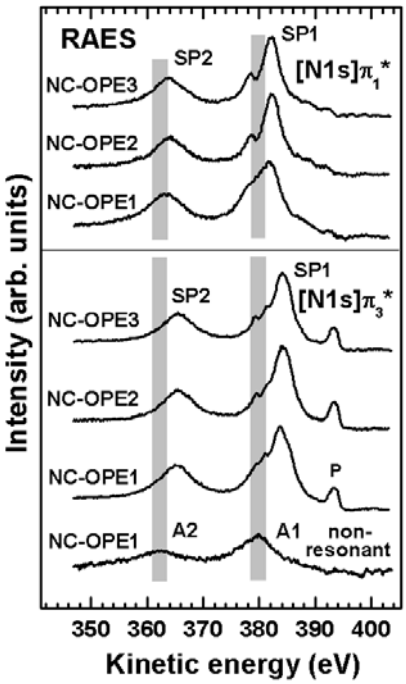
RAES
SP2
SP1
[N1s]π1*
NC-OPE3
NC-OPE2
NC-OPE1
SP1
[N1s]π3*
SP2
NC-OPE3
NC-OPE2
NC-OPE1
P
NC-OPE1
A2
A1
non-
resonant
Intensity (arb. units)
350 360 370 380 390 400
Kinetic energy (eV)

Figure 3

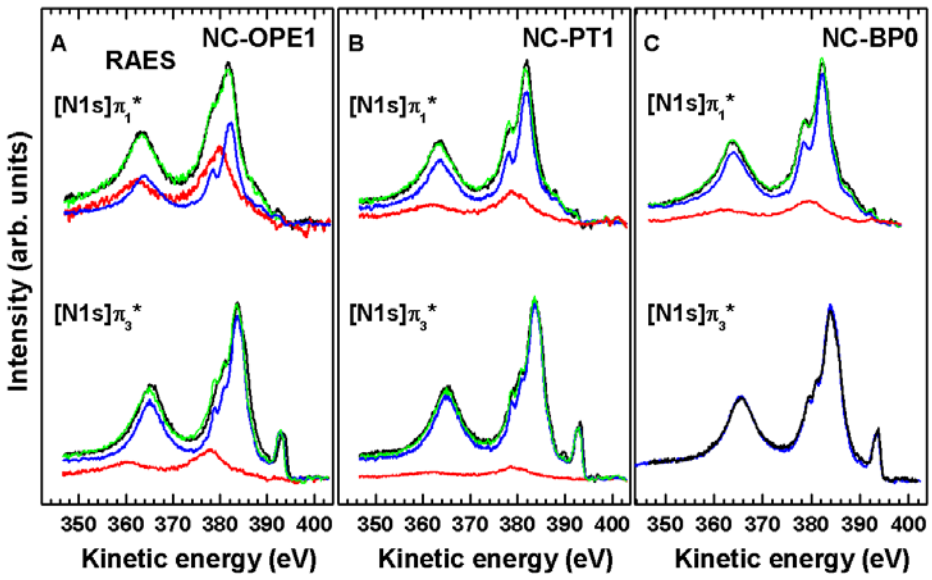
A
RAES
NC-OPE1
[N1s]π1*
[N1s]π3*
B
NC-PT1
[N1s]π1*
[N1s]π3*
C
NC-BP0
[N1s]π1*
[N1s]π3*
Intensity (arb. units)
350 360 370 380 390 400
Kinetic energy (eV)
350 360 370 380 390 400
Kinetic energy (eV)
350 360 370 380 390 400
Kinetic energy (eV)

Figure 4